FBXO22 promotes hepatocellular carcinoma progression via paracrine myo-inositol-induced M2-type polarization of macrophages

LIANGLIANG BAI[1*], JING XIONG[2*], SIHAI CHEN[1*], JIAHAO HU[1], MEIXIA ZHANG[1], BIMIN LI[1], JING HU[3] and MINGYAN HE[1]

[1]Department of Gastroenterology, Jiangxi Provincial Key Laboratory of Digestive Diseases, Jiangxi Clinical Research Center for Gastroenterology, Digestive Disease Hospital, The First Affiliated Hospital, Jiangxi Medical College, Nanchang University, Nanchang, Jiangxi 330006, P.R. China; [2]Department of General Practice, The First Affiliated Hospital, Jiangxi Medical College, Nanchang University, Nanchang, Jiangxi 330006, P.R. China; [3]Department of Cardiology, Jiangxi Provincial People's Hospital, The First Affiliated Hospital of Nanchang Medical College, Nanchang, Jiangxi 330200, P.R. China

Received May 7, 2025; Accepted November 3, 2025

DOI: 10.3892/ijmm.2025.5707

Abstract. Macrophages play a key role in hepatocellular carcinoma (HCC) progression, but the mechanisms underlying this involvement remain unclear. In the present study, mice with HCC were used for *in vivo* experiments, and 97H and THP-1 cells were used for *in vitro* experiments. Metabolomic analysis was performed to detect changes of metabolites in the supernatant of 97H cells. Flow cytometry and immunohistochemical staining were performed to assess macrophage polarization. Western blotting was performed to examine the levels of phosphorylated (p-) PI3K, p-AKT and NRF2. Reverse transcription-quantitative polymerase chain reaction was performed to examine *FBXO22*, *IMPA1* and *PTEN* mRNA expression levels. FBXO22 significantly promoted the release of myo-inositol in the cell supernatant of 97H cells, markedly decreased the number of CD86-positive cells (M1 macrophages), and increased the number of CD206-positive cells (M2 macrophages) in both THP-1 cells and mouse HCC tumor tissues. The promoting effect of myo-inositol on M2 macrophages was reversed by transfection with small interfering (si)-*SLC5A3 in vitro*. In addition, FBXO22 overexpression reduced PTEN protein levels and then elevated NRF2 protein levels upregulating IMPA1 and inducing myo-inositol release in 97H cells. Co-culturing of 97H and THP-1 cells revealed that the stimulatory effect of 97H cells transfected with an overexpression (oe)-*FBXO22* construct on M2 macrophages was reversed by co-transfection with the si-*IMPA1*. Co-immunoprecipitation revealed a promoting effect of FBXO22 on PTEN ubiquitination via direct interaction in 97H cells. Furthermore, luciferase activity and chromatin immunoprecipitation assays indicated direct transcriptional regulation of IMPA1 expression by NRF2 in 97H cells. The *in vivo* experiments further revealed that transfection with the si-*IMPA1* reversed the promoting effect of oe-*FBXO22* on tumor growth and M2 polarization by reducing myo-inositol levels in tumor tissues. In conclusion, FBXO22 degrades PTEN by inducing its ubiquitination to elevate NRF2 protein levels. As a result, IMPA1 expression is increased, which causes myo-inositol release by HCC cells and further induces M2-type macrophages via SLC5A3 to promote HCC tumor growth. The present study identified a novel molecular mechanism by which FBXO22 promotes HCC progression.

Correspondence to: Dr Mingyan He, Department of Gastroenterology, Jiangxi Provincial Key Laboratory of Digestive Diseases, Jiangxi Clinical Research Center for Gastroenterology, Digestive Disease Hospital, The First Affiliated Hospital, Jiangxi Medical College, Nanchang University, 17 Yongwaizheng Street, Nanchang, Jiangxi 330006, P.R. China
E-mail: ndyfy05035@ncu.edu.cn

*Contributed equally

Key words: FBXO22, myo-inositol, macrophages, hepatocellular carcinoma

Introduction

Hepatocellular carcinoma (HCC) is the fourth leading cause of cancer death worldwide, and despite the wide application of surgical resection, radiation therapy and molecular targeted therapy for HCC treatment, its prognosis remains poor, seriously threatening people's life and health (1,2). The 5-year survival rate of patients with HCC is 5-30%, and extrahepatic metastasis is the main cause of death. Therefore, it is urgently necessary to elucidate in detail the pathological mechanisms of HCC and explore novel treatments.

The tumor microenvironment (TME) is composed of various elements, such as macrophages, fibroblasts and extracellular stroma, which are closely associated with tumor progression and metastasis (3,4). Macrophages play a key role in tumor progression, and numerous studies reported that various changes in the TME result in the transformation of

M2-type macrophages, namely tumor-associated macrophages (TAMs) (5). A large number of TAMs infiltrating the TME often indicates poor prognosis in patients with cancer (6,7). However, the exact mechanisms that change macrophage phenotypes remain unclear. Although tumor cells regulate macrophage function via direct cellular contact with cell membrane ligands and integrin signaling, there is evidence that paracrine factors released by tumor cells are major contributors to immune microenvironment remodeling. HCC-derived cytokines and growth factors such as C-C motif chemokine ligand 2, transforming growth factor beta, macrophage migration inhibitory factor and hepatocyte growth factor are essential for macrophage recruitment and differentiation (8). High-mobility group box 1 protein derived from HCC cells induces M2 macrophage polarization (9). Thus, exploring the molecular crosstalk between tumor cells and macrophages in HCC may provide clues for a novel treatment strategy.

As an important part of the Skp1-Cullin1-F-box (SCF) E3 ubiquitination complex, F-box affects numerous biological processes in cells, such as cell cycle, immune regulation and signal transduction (10,11). Ubiquitination induces the degradation of the proteasome, thus promoting or inhibiting the occurrence and metastasis of tumors. F-box only protein 22 is an F-box protein encoded by the *FBXO22* gene located on human chromosome 15q24.2. FBXO22 binds to histone lysine demethylase 4A (KDM4A) and regulating its homeostasis, whereas KDMA4 affects genome replication and stability, that is, parameters that may be associated with tumorigenesis (12). In addition, FBXO22 mediates the degradation of Kruppel-like factor 4 and thereby promotes HCC progression (13). However, the effects of FBXO22 on macrophages in HCC remain unclear. Thus, in the present study, it was investigated whether FBXO22 facilitates HCC progression by regulating macrophages via the modulation of the release of paracrine factors by tumor cells.

Materials and methods

Cell culture. MHCC97-H (97H) cells, obtained from Shanghai Yaji Biotechnology Co., Ltd. (cat. no. YS-C258), were cultured in Dulbecco's modified Eagle's medium (cat. no. G4511; Wuhan Servicebio Biotechnology Co., Ltd.) at 37˚C in the atmosphere of 95% air and 5% CO_2. Trypsin (0.25%) was used for digestion when the cells reached 70-80% confluence. THP-1 cells (cat. no. YS-C361; Shanghai Yaji Biotechnology Co., Ltd.) were cultured in the RPMI-1640 medium (cat. no. G4538; Wuhan Servicebio Biotechnology Co., Ltd.) at 37˚C in the atmosphere of 95% air and 5% CO_2. Both cell lines were collected for subsequent experiments in the logarithmic growth phase after three passages. 97H and THP-1 cells were examined for short tandem repeats, and both were found not to be contaminated with other cells. In addition, both 97H and THP-1 cells tested negative for mycoplasma.

Cell transfection and treatment. 97H cells were firstly transfected with the overexpression (oe)-FBXO22 or oe-NC lentivirus (MOI=10; OligoBio) for 72 h at 37˚C to establish 97H-NC or 97H-FBXO22 cells, and then 97H-NC or 97H-FBXO22 cells were transfected with small interfering (si)-IMPA1 or si-NC mRNAs (20 μM; OligoBio) for 48 h at 37˚C, respectively. Also, 97H-NC or 97H-FBXO22 cells were treated with cycloheximide (CHX; 200 μg/ml; cat. no. HY-12320; MedChemExpress) for different periods (2, 4 and 8 h) or MG132 (10 μM; cat. no. HY-13259; MedChemExpress) for 12 h. The THP-1 cells were transfected with the si-NC or si-SLC5A3 mRNAs (20 μM; OligoBio) for 48 h at 37˚C. All the transfections were performed via Lipofectamine 2000 (cat. no. 11668027; Invitrogen; Thermo Fisher Scientific, Inc.). A total of 24 h later, the transfected cells were harvested for the following experiments. The siRNA sequences were as follows: si-*IMPA1*: 5'-GAAUGUUAUGCUGAAAAGUUC-3'; si-*SLC5A3*-1: 5'-GCACUUACACUUAUGAUUAUU-3'; si-*SLC5A3*-2: 5'-GCAAGUUAAAGUAAUACUAAA-3'; si-*SLC5A3*-3: 5'-GUGACUUAGACUCUAUCUUUA-3'; and si-NC: 5'-ACGUGACACGUUCGGAGAATT-3'.

Co-culture of 97H and THP-1 cells. 97H cells were transfected with oe-*FBXO22* lentivirus or si-*IMPA1* and added to the upper compartment of Transwell chambers after 24 h. Then, the THP-1 cells were added to the lower compartment and co-cultured with the 97H cells transfected with oe-*FBXO22* or si-*IMPA1* and cultured in the upper compartment for 24 h; the ratio of 97H/THP-1 cells was 1:2, whereupon the cells were collected for flow cytometric analysis.

Flow cytometry. THP-1 cells ($1x10^6$ cells/100 μl) were stained with a FITC-labelled anti-human CD86 antibody (cat. no. 374203; 1:20; BioLegend, Inc.) or a PE-labelled anti-human CD206 antibody (cat. no. 321105; 1:20; BioLegend, Inc.) for 30 min at room temperature and analyzed using a BD FACSCalibur flow cytometer (BD Biosciences) and FlowJo software version 10.8.1 (FlowJo LLC).

Cell viability. THP-1 cells ($2x10^3$ cells/100 μl) were seeded into a 96-well plate, Cell Counting Kit-8 reagent (10 μl; Beyotime Institute of Biotechnology) was added to each well, and the cells were incubated for 3 h at 37˚C in the dark. The optical density of each well was measured at 450 nm using a microplate reader (SpectraMax i3x; Molecular Devices, LLC).

Dual luciferase reporter assay. The *IMPA1* 3'-untranslated region (UTR) containing wild or mutant binding sites was cloned into the psiCHECKTM-2 vector, and 293T cells (cat. no. CL-0005; Life Science & Technology Co., Ltd.) were co-transfected with oe-*NRF2* and *IMPA1* 3'-UTR psiCHECKTM-2 plasmid for 48 h via Lipofectamine 2000 (cat. no. 11668027; Invitrogen; Thermo Fisher Scientific, Inc.). The cells were then harvested and washed with phosphate-buffered saline (PBS), and luciferase activity was measured using a dual luciferase reporter assay system (cat. no. E1910; Promega Corporation). For statistical analysis, *Renilla* fluorescence value, firefly fluorescence value, and the background fluorescence value were read, respectively. Firefly was the internal control. The relative luciferase activity was calculated as follows: (*Renilla*-background)/(firefly-background).

Reverse transcription-quantitative polymerase chain reaction (RT-qPCR). Total RNA was extracted using an RNA Extraction Kit (cat. no. R1200; Yuduobio), and reverse transcribed into complementary DNA using a reverse transcription kit (Aidlab

Biotechnology Co., Ltd.) following the manufacturer's instructions. RT-qPCR was performed using an ABI-7500 Real-Time PCR System (Applied Biosystems; Thermo Fisher Scientific, Inc.) with genes primers and SYBR Green PCR Master Mix (Tiangen Biotech Co., Ltd.). PCR amplification conditions were as follows: 94˚C for 10 min, (94˚C for 20 sec, 55˚C for 20 sec, 72˚C for 20 sec) for 40 cycles. The data were analyzed using the $2^{-\Delta\Delta Cq}$ method as previously described (14), and β-actin (*ACTB*) mRNA level was used for the normalization of expression data. The following primers were used: *SLC5A3* forward, 5'-AGCACCGTGAGTGGATACTTC-3' and reverse, 5'-CCCTGACCGGATGTAAATTGG-3'; *IMPA1* forward, 5'-TAACTCTAGCAAGACAAGCTGGA-3' and reverse, 5'-TCAACTTTTTGGTCCGTAGCAG-3'; and *ACTB* forward, 5'-AGCGAGCATCCCCCAAAGTT-3' and reverse, 5'-GGG CACGAAGGCTCATCATT-3'.

Western blot analysis. The cells were lysed via RIPA lysis buffer (cat. no. G2008; Wuhan Servicebio Biotechnology Co., Ltd), and the protein content was determined using a bicinchoninic acid (BCA) protein assay kit (cat. no. E112; Vazyme Biotech Co., Ltd.). The equal amount (40 μg per lane) of protein was separated using 10% SDS-polyacrylamide gels, and then the protein was transferred onto a nitrocellulose membrane. The membrane was maintained with 5% non-fat milk for 1 h at room temperature, and incubated with the primary antibodies against the following proteins: PI3K (1:10,000; cat. no. 67071-1-Ig; Proteintech Group, Inc.), phosphorylated (p-) PI3K (1:1,000; cat. no. AF3242; Affinity Biosciences), AKT1 (1:10,000; cat. no. 80457-1-RR; Proteintech Group, Inc.), p-AKT1 (1:5,000; cat. no. 80462-1-RR, Proteintech Group, Inc.), FBXO22 (1:2,000; cat. no. 13606-1-AP; Proteintech Group, Inc.), IMPA1 (1:300; cat. no. 16593-1-AP; Proteintech Group, Inc.), SLC5A3 (1:1,000; cat. no. DF4521; Affinity Biosciences), PTEN (1:5,000; cat. no. 60300-1-Ig; Proteintech Group, Inc.), and NRF2 (1:2,000; cat. no. 16396-1-AP; Proteintech Group, Inc.). β-actin protein level was the internal control. Horseradish peroxidase-conjugated goat anti-mouse IgG (1:3,000; cat. no. SA00001-1-A; Proteintech Group, Inc.) served as the secondary antibody. Finally, an enhanced chemiluminescence kit (Vazyme Biotech Co., Ltd.) was utilized to determine the protein bands, and the optical density was analyzed using the Image-Pro Plus 6.0 software (Media Cybernetics, Inc.).

Bioinformatics analysis. Based on the TIMER database (https://compbio.cn/timer3/), the correlation between FBXO22 and macrophages in HCC was predicted.

Co-immunoprecipitation (co-IP). Co-IP assays were performed using an IP kit (cat. no. P2179S; Beyotime Institute of Biotechnology). 97H cells were lysed in RIPA lysis buffer including phenyl-methane-sulfonyl fluoride, followed by the incubation with an anti-NRF2 (1:2,000) or anti-PTEN antibody (1:5,000) at 4˚C overnight, and IgG served as negative control. Then the mixture of the lysis buffer (500 μl), the antibodies (1 μg), and protein A+G magnetic beads (30 μl) was incubated at 4˚C for 4 h, and was separated using a magnetic rack. Then the obtained magnetic beads were washed using PBS for 5 times, and 40 μl of 1X loading buffer was added. The magnetic beads were boiled for 10 min in a 98˚C metal bath, and then were centrifuged at 13,000 rpm for 3 min, and beads with bound protein were removed, and the targeted protein was tested using western blotting.

Chromatin immunoprecipitation (ChIP). The ChIP assay was performed to analyze the interaction between NRF2 and IMPA1 using a Pierce Agarose ChIP kit (cat. no. 26156; Thermo Fisher Scientific, Inc.). Briefly, homogenates of 97H cells transfected with oe-NC or oe-*FBXO22* were sonicated to generate short fragments of genomic DNA, and equal amounts of treated chromatin were added to microwells containing an anti-NRF2 antibody. Then, cross-linked DNA was released from the antibody-captured protein-DNA complex, and purified DNA was used for PCR analysis.

Liquid chromatography tandem-mass spectrometry (LC-MS/MS). 97H cells transfected with oe-NC or oe-*FBXO22* were used for non-targeted metabolomic analysis by Bioprofile (www.bioprofile.cn/bxdx/list.aspx). Briefly, metabolomics profiling was analyzed using a UPLC-ESI-Q-Orbitrap-MS system (UHPLC; Shimadzu Nexera X2 LC-30AD; Shimadzu) coupled with Q-Exactive Plus (Thermo Fisher Scientific, Inc.). The electrospray ionization (ESI) with positive-mode and negative mode were applied for MS data acquisition separately. The ESI source conditions were set as follows: Spray Voltage: 3.8 kv (positive) and 3.2 kv (negative); Capillary Temperature: 320˚C; Sheath Gas (nitrogen) flow: 30 arb (arbitrary units); Aux Gas flow: 5 arb; Probe Heater Temp: 350˚C; S-Lens RF Level: 50. The instrument was set to acquire over the m/z range 70-1050 Da for full MS. The full MS scans were acquired at a resolution of 70,000 at m/z 200, and 17,500 at m/z 200 for MS/MS scan. The maximum injection time was set to for 100 ms for MS and 50 ms for MS/MS. The isolation window for MS2 was set to 2 m/z and the normalized collision energy (stepped) was set as 20, 30 and 40 for fragmentation. For statistical analysis, variable importance in projection (VIP) value >1 was the initial screening criterion to identify metabolites differentially expressed between 97H cells transfected with oe-NC or oe-*FBXO22*, and univariate statistical analysis ($P<0.05$) was further employed to determine whether the levels of metabolites were significantly different.

Establishment of a xeno-transplanted tumor model and experimental groups. 97H cells were resuspended in PBS to prepare cell suspension ($5x10^7$ cells/ml), and then HCC was induced by a subcutaneous injection of 97H cell suspension (100 μl/mouse) into the thigh of 3-5-week old male BALB/C nude mice (Cavens Laboratory Animal). Before the experiments, mice were acclimated for 1 week. All mice (n=30; 11-15 g) were provided free and unlimited access to normal chow and water, housed under suitable temperature (22±2˚C) and humidity (65±5%) with a 12/12-h light/dark cycle. The model mice were randomly divided into six groups (n=4): control, myo-inositol (this group received 200 mg/ml myo-inositol intra-gastrically) (15,16), 97H-NC + si-NC (this group received a subcutaneous injection of 97H-NC cells followed by intratumoral injections of si-NC once weekly for 2 weeks), 97H-FBXO22 + si-NC group (this group received a subcutaneous injection of 97H-FBXO22 cells followed by

intratumoral injections of si-NC once weekly for 2 weeks), 97H-NC + si-IMPA1 (this group received a subcutaneous injection of 97H-NC cells followed by intratumoral injections of si-IMPA1 once weekly for 2 weeks), 97H-FBXO22 + si-IMPA1 (this group received a subcutaneous injection of 97H-FBXO22 cells followed by intratumoral injections of si-IMPA1 once weekly for 2 weeks). Tumor growth was monitored every 3 days for ~3 weeks. A total of 21 days later, the mice were euthanized using the cervical dislocation under the inhalation anesthesia of isoflurane. Briefly, mice were put in the desiccator with isoflurane (3.0%), and shook the desiccator after 3 min, if the mouse turned to a lateral position and did not attempt to return to its lying position, indicating that the mouse has been fully anesthetized. Then isoflurane (1.5%) was used for maintaining anesthesia, and the mouse did not respond when its tail, toes, or the cornea was touched, then a laboratory professional quickly performed cervical dislocation, and which should be as fast as possible to reduce mouse pain. The present study adhered to the recommendations outlined in the ARRIVE Guidelines 2.0 and was approved by the Institutional Animal Care and Use Committee of the First Affiliated Hospital, Jiangxi Medical College, Nanchang University (approval no. CDYFY-IACUC-202501GR136; Nanchang, China).

Immunohistochemistry (IHC) staining. After the fixation with 4% polyformaldehyde liquid for 24 h at 4˚C, dehydration and transparency, the tumor tissues were embedded in paraffin and cut into 5-μm sections. The sections were incubated with 3% hydrogen peroxide (Thermo Fisher Scientific, Inc.) at room temperature for 8 min and blocked with 10% goat serum (cat. no. 16210064; Gibco; Thermo Fisher Scientific, Inc.) at room temperature for 30 min. Then the sections were incubated with anti-CD86 (1:100; cat. no. 19589S; Cell Signaling Technology, Inc.) or anti-CD206 (1:200; cat. no. 24595S; Cell Signaling Technology, Inc.) antibodies at 4˚C overnight and horseradish peroxidase-conjugated goat anti-mouse IgG (1:200; cat. no. S0002; Affinity Biosciences) at room temperature for 30 min. Then the sections were stained with 3,3'-diaminobenzidine and hematoxylin at room temperature for 10 min. Finally, images of the sections were captured using an inverted fluorescence microscope (Olympus Corporation).

Statistical analysis. Differences between groups were analyzed by the unpaired Student's t-test or one-way analysis of variance (ANOVA) using GraphPad Prism 7.0 (GraphPad Software; Dotmatics), followed by Tukey's post hoc test. The Brown-Forsythe test was used to assess variance homogeneity in ANOVA. $P<0.05$ was considered to indicate a statistically significant difference.

Results

FBXO22-induced myo-inositol release by 97H cells promotes M2 polarization of THP-1 cells. Results of non-targeted metabolomic analysis of 97H cells transfected with oe-NC or oe-*FBXO22* and hierarchical clustering of the top 50 differential metabolites (VIP >1) are illustrated in Fig. 1. Based on human metabolome database HMDB-HU, out of the top six metabolites ($P<0.01$; Fig. 1; Table I), myo-inositol and R-3-hydroxydodecanoic acid were selected for further validation, owing to their commercial availability. Both RT-qPCR and western blot analyses revealed that, compared with R-3-hydroxydodecanoic acid, myo-inositol exhibited the best promoting effect on Arg1 expression and inhibitory effect on inducible nitric oxide synthase expression in THP-1 cells (Fig. S1A and B); thus, myo-inositol was selected for the following experiments. Then, the effects of myo-inositol on macrophages were investigated. Myo-inositol did not significantly affect cell viability (Fig. 2A). Flow cytometry revealed that myo-inositol significantly reduced the number of CD86-positive THP-1 cells and increased the number of CD206-positive THP-1 cells (Fig. 2B and C). In addition, myo-inositol significantly increased p-PI3K and p-AKT levels in THP-1 cells (Fig. 2D and E). Based on the results illustrated in Figs. 1, 2 and S1, it was concluded that *FBXO22* overexpression induces the release of myo-inositol in 97H cells and further promotes M2 polarization of macrophages.

Myo-inositol promotes M2 polarization of THP-1 cells via SLC5A3. SLC5A3 transports myo-inositol from the outside to the inside of the cells; thus, the role of SLC5A3 in the stimulatory effect of myo-inositol on M2 polarization of THP-1 cells was explored. First, three si-*SLC5A3* siRNAs were used to silence *SLC5A3* expression in THP-1 cells, and si-*SLC5A3*-2 was selected because of its high knockdown efficiency (Fig. 3A and B). Flow cytometric analysis revealed that the marked reduction in CD86-positive cells and increase in CD206-positive cells induced by myo-inositol were reversed by si-*SLC5A3* in THP-1 cells (Fig. 3C and D). Western blot analysis revealed that increased p-PI3K and p-AKT levels induced by myo-inositol in THP-1 cells were significantly reversed by the incubation with si-*SLC5A3* (Fig. 3E and F). These results suggested that SLC5A3 promotes the effect of myo-inositol on M2 polarization of THP-1 cells.

FBXO22-induced myo-inositol release promotes M2 polarization of THP-1 cells via the PTEN/NRF2/IMPA1 axis. Actually, in our preliminary experiments, the TIMER database revealed that FBXO22 is positively correlated with M2 macrophages in HCC (Fig. S2). Thus, the mechanisms by which FBXO22-induced myo-inositol release promoted M2 polarization were explored. It was found that transfection with oe-*FBXO22* significantly upregulated *FBXO22* mRNA expression and protein level (Fig. 4A, C and D), *IMPA1* mRNA expression and protein level (Fig. 4B, C and E), and myo-inositol release (Fig. 4F) in 97H cells. In addition, transfection with oe-*FBXO22* did not affect *PTEN* mRNA expression (Fig. 4G) but significantly reduced PTEN protein level (Fig. 4H) in 97H cells. The use of CHX and proteasome inhibitor MG132 further confirmed that FBXO22 degraded PTEN, reducing PTEN protein level (Fig. 4I-K). Furthermore, co-IP analysis revealed an interaction between FBXO22 and PTEN (Fig. 4L) and the promoting effect of FBXO22 on PTEN ubiquitination (Fig. 4M) in 97H cells.

In addition, co-IP analysis demonstrated a direct interaction between PTEN and NRF2 in 97H cells (Fig. 5A). Western blot analysis showed that treatment with oe-*FBXO22* significantly upregulated NRF2 protein levels in 97H cells (Fig. 5B). The luciferase assay revealed that NRF2 bound to the promoter

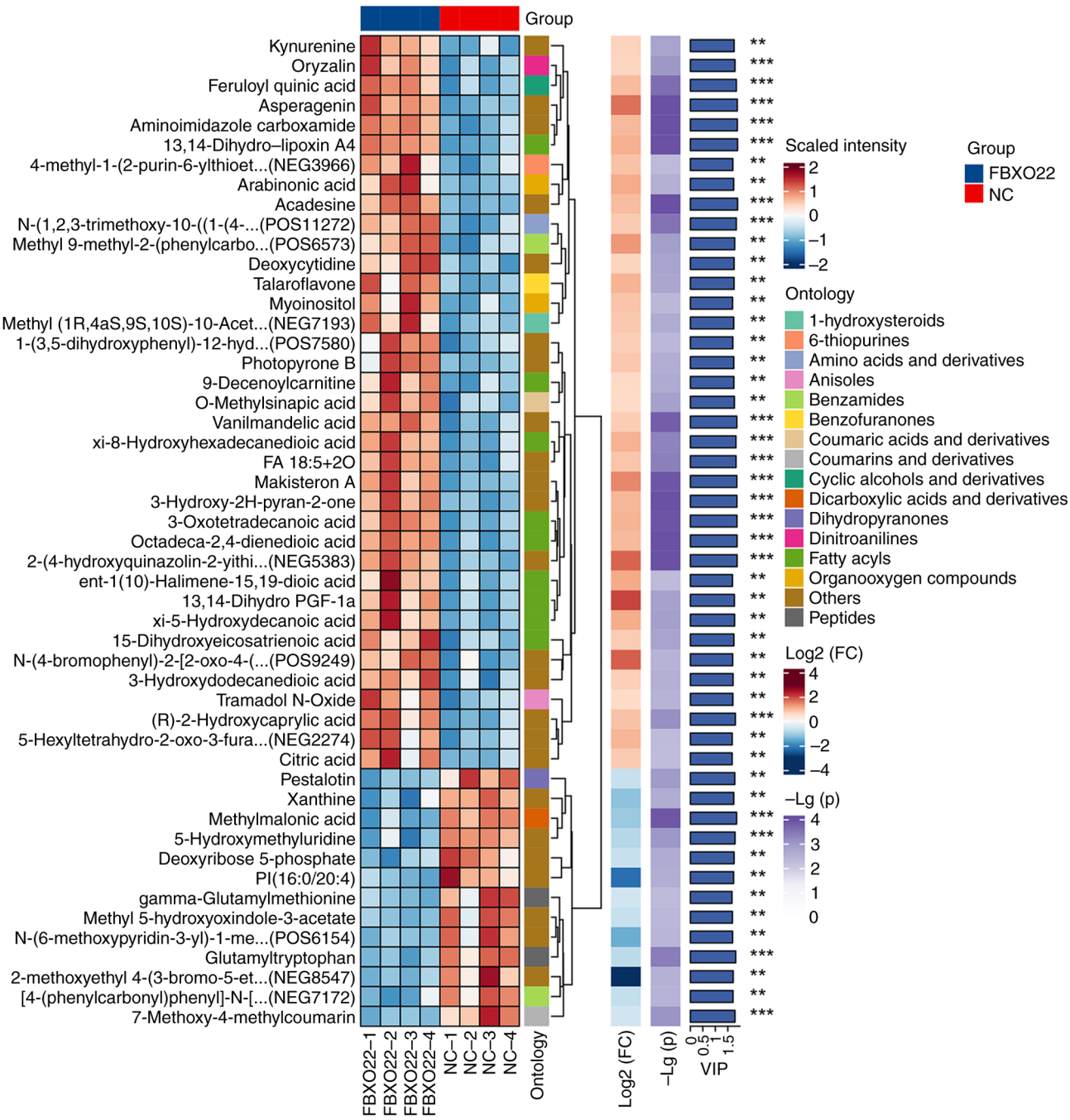

Figure 1. Detection of differentially expressed metabolites in 97H cells overexpressing *FBXO22*. 97H cells were transfected with oe-*FBXO22*, and cell supernatants were collected for non-target metabolomic analysis. Hierarchical clustering results of the top 50 differential metabolites (VIP >1) are illustrated. **P<0.01, ***P<0.001. Oe-, overexpression.

region of *IMPA1* mRNA to promote *IMPA1* transcription in 293T cells (Fig. 5C). The ChIP assay further showed the direct transcriptional regulation of *IMPA1* by NRF2 in 97H cells (Fig. 5D). Furthermore, transfection with oe-*FBXO22* significantly increased *IMPA1* mRNA expression and protein level (Fig. 5E and F) and myo-inositol release (Fig. 5G) in 97H cells, the changes that were markedly reversed by the treatment with si-*IMPA1*. Flow cytometric analysis also demonstrated that co-transfection with *si-IMPA1* significantly reversed the decrease in CD86-positive cells and increase in CD206-positive cells induced in 97H cells by transfection with oe-*FBXO22* (Fig. 5H and I). These results suggested that FBXO22 degrades PTEN by promoting PTEN ubiquitination, which upregulates NRF2 protein levels and stimulates IMPA1 to induce myo-inositol release by 97H cells, thus promoting M2 polarization of THP-1 cells.

Myo-inositol promotes tumor growth and induces M2 polarization in HCC mice. Finally, the effect of myo-inositol was assessed *in vivo*. The tumor volume in the myo-inositol group was significantly larger compared with that in the PBS group (Fig. 6A and B). In addition, treatment with myo-inositol significantly increased p-PI3K and p-AKT levels (Fig. 6C and D), reduced the number of CD86-positive cells, and increased

Table I. Metabolites in Fig. 1 that were annotated to the human metabolome database HMDB-HU.

Alignment ID	Metabolite name	BLOCKID	P-value	FC
NEG5475	13,14-Dihydro- lipoxin A4	HMDB-HU-SE-N207	3.60E-05	2.093572
POS6421	9-Decenoylcarnitine	HMDB-HU-SE-P86	0.002324526	1.522776
NEG1282	Arabinonic acid	HMDB-HU-UR-N167	0.002978637	2.182012
NEG1549	Myo-inositol	HMDB-HU-SE-N114	0.004211906	1.812636
NEG5087	ent-1(10)-Halimene-15,19-dioic acid	HMDB-HU-SE-N494	0.004829203	2.215659
NEG2332	(R)-3-Hydroxydodecanoic acid	HMDB-HU-SE-N152	0.007715954	3.134245
NEG4975	5,8,12-Trihydroxy-9-octadecenoic acid	HMDB-HU-SE-N261	0.011872046	2.293262
NEG5058	Bicyclo-Prostaglandin E2	HMDB-HU-SE-N901	0.01287796	1.65443
POS7620	Tetradeca-5,7,9-trienoylcarnitine	HMDB-HU-UR-P525	0.014604632	1.581081
NEG332	Citraconic anhydride	HMDB-HU-UR-N65	0.023404697	1.500645
NEG4602	Octadecenedioic acid	HMDB-HU-SE-N1015	0.039284274	1.509278
POS5061	Creatine riboside	HMDB-HU-UR-P452	0.046645468	1.579277
POS4124	Butenylcarnitine	HMDB-HU-SE-P75	0.062279284	1.838155
POS434	1-Pyrrolidinecarboxaldehyde	HMDB-HU-SE-P259	0.062433302	1.738346
POS2353	Homoarecoline	HMDB-HU-SE-P283	0.100541459	2.153713
NEG8112	Taurohyocholate	HMDB-HU-SE-N52	0.112350153	1.548636
POS2183	Dimethylamphetamine	HMDB-HU-SE-P297	0.191678682	1.517535

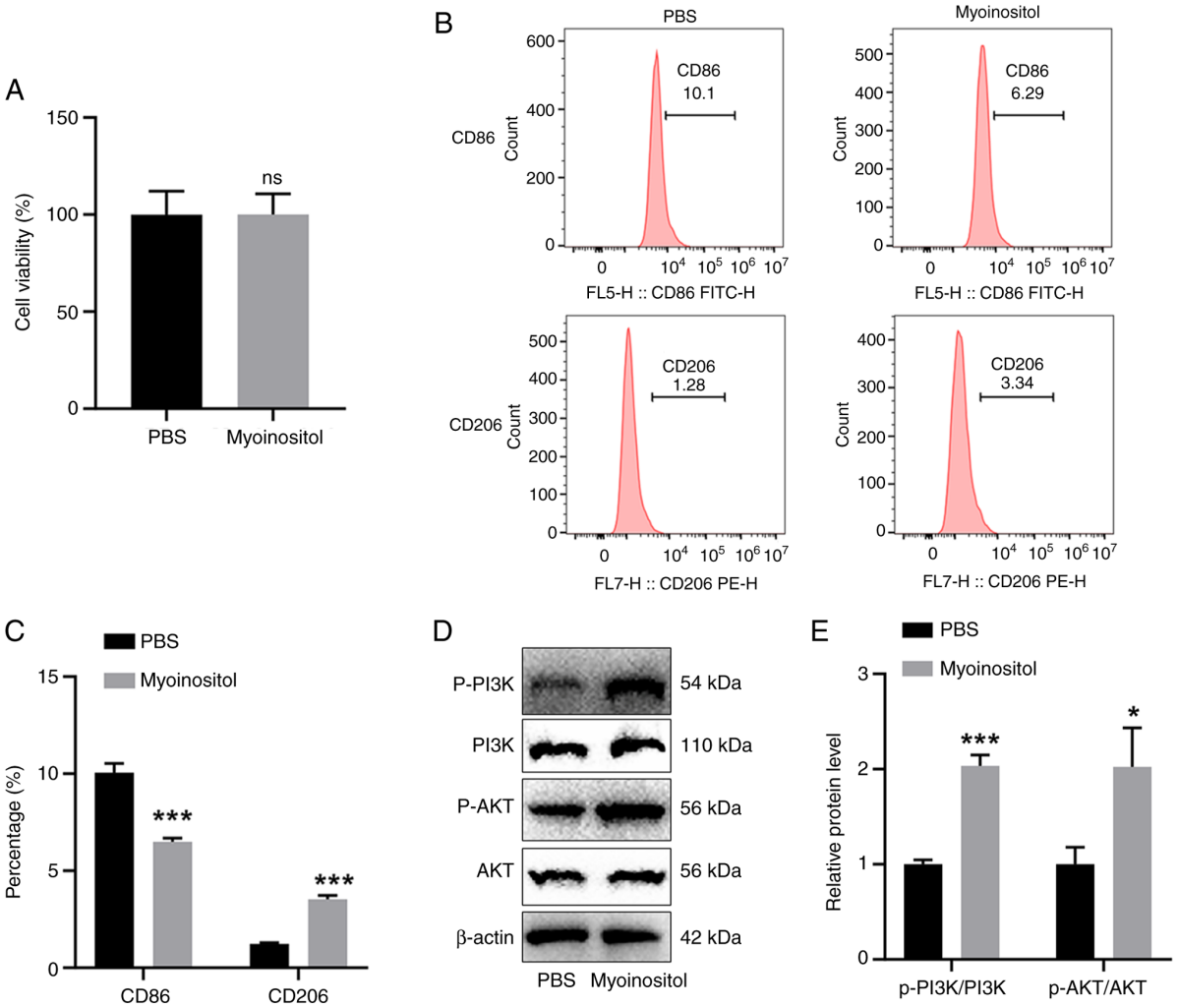

Figure 2. FBXO22-induced myo-inositol release promotes M2 polarization of THP-1 cells. 97H cells were treated with myo-inositol. (A) A Cell Counting Kit-8 assay was performed to assess cell viability. (B and C) Flow cytometry was performed to detect CD86- and CD206-positive THP-1 cells. (D and E) Western blotting was performed to examine p-PI3K and p-AKT levels in THP-1 cells. *P<0.05 and ***P<0.001. p-, phosphorylated.

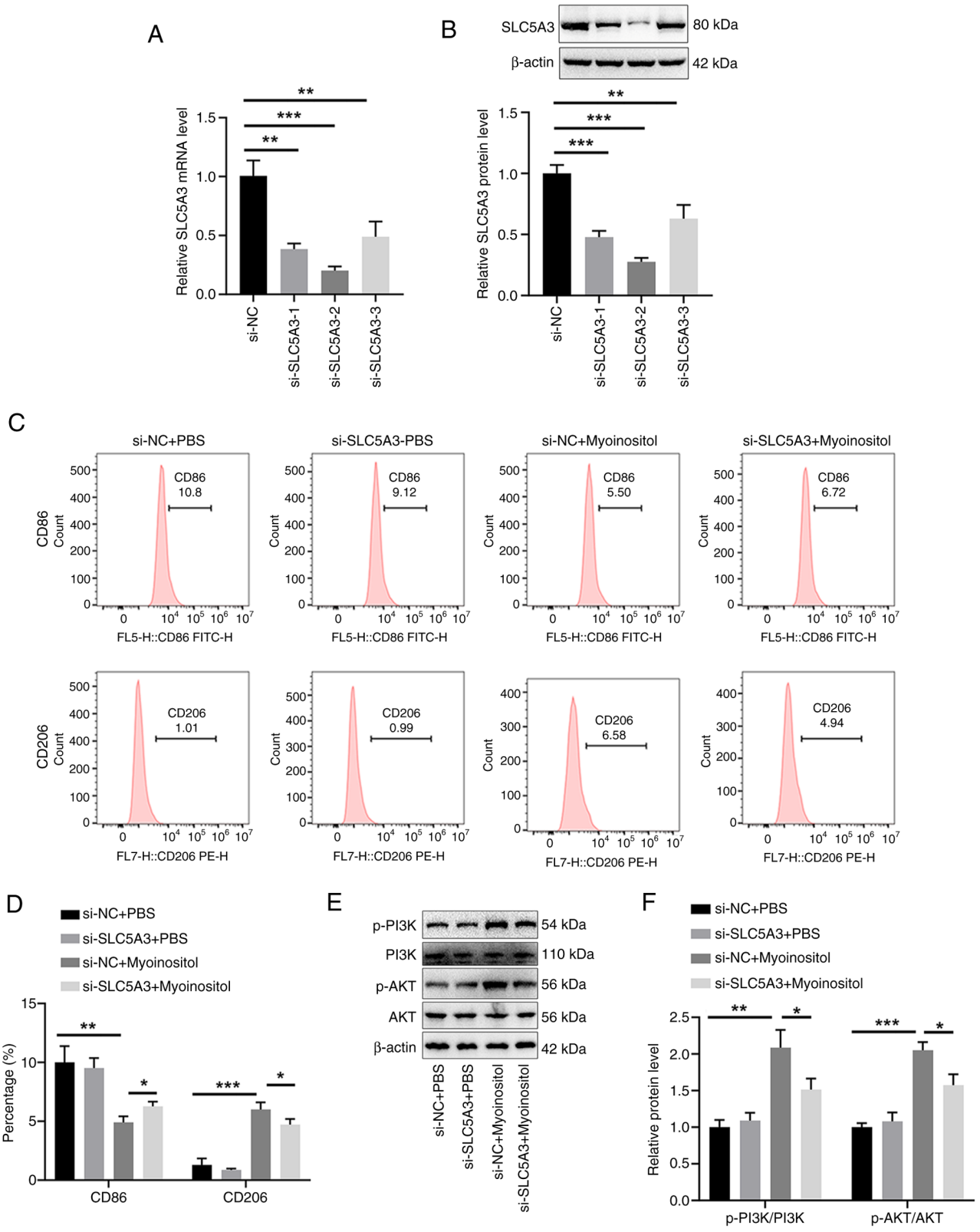

Figure 3. Myo-inositol induces M2 polarization of THP-1 cells via SLC5A3. THP-1 cells were transfected with si-*SLC5A3*. (A) Reverse transcription-quantitative PCR and (B) western blotting were performed to detect SLC5A3 expression. THP-1 cells were transfected with si-*SLC5A3*, followed by treatment with 10 μM myo-inositol. (C and D) Flow cytometry was performed to detect CD86-positive and CD206-positive THP-1 cells. (E and F) Western blotting was performed to examine p-PI3K and p-AKT levels in THP-1 cells. *P<0.05, **P<0.01 and ***P<0.001. p-, phosphorylated.

the number of CD206-positive cells in HCC tumor tissues (Fig. 6E and F). These results suggested that myo-inositol promotes HCC progression *in vivo*.

FBXO22 promotes tumor growth and induces M2 polarization via IMPA1 in HCC mice. Furthermore, *FBXO22* overexpression significantly increased tumor volume (Fig. 7A and B),

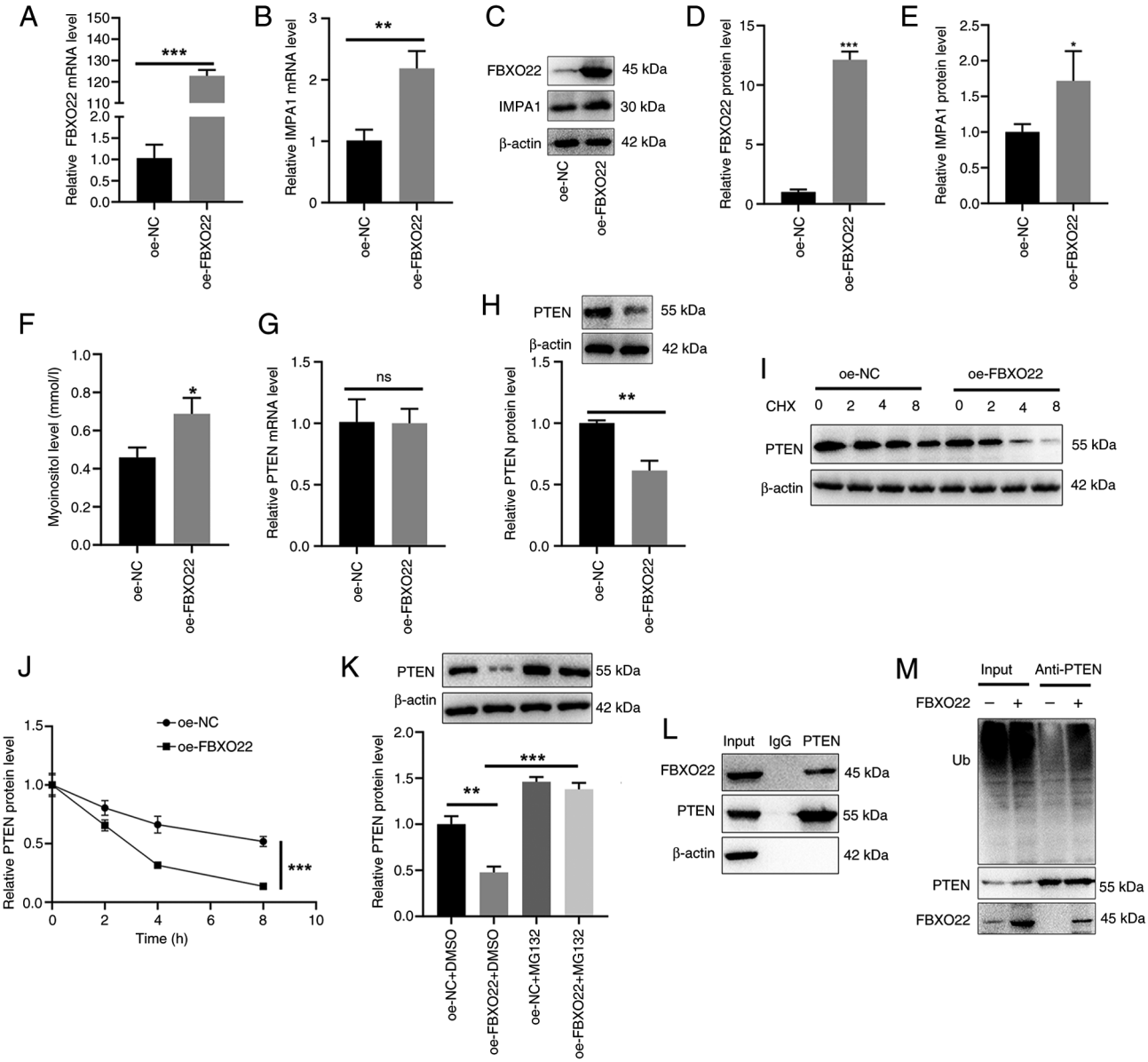

Figure 4. FBXO22 induces PTEN ubiquitination and subsequent degradation in THP-1 cells. 97H cells were transfected with oe-*FBXO22*. Reverse transcription-quantitative PCR and western blotting were performed to detect mRNA expression levels and protein levels of (A, C and D) *FBXO22*, (B, C and E) *IMPA1* and (G and H) *PTEN*. (F) A myo-inositol detection kit was used to detect myo-inositol in cell supernatants. (I and J) 97H cells were transfected with oe-*FBXO22*, followed by the treatment with CHX (200 μg/ml) for different periods (2, 4 and 8 h). Western blotting was performed to detect PTEN protein levels. (K) 97H cells were transfected with oe-*FBXO22* followed by the treatment with MG132 (10 μM) for 12 h. Western blotting was performed to detect PTEN protein levels. (L) 97H cells were incubated with an anti-PTEN antibody, and western blotting was performed to detect FBXO22 protein levels. (M) 97H cells were incubated with an anti-PTEN antibody, followed by the transfection with oe-*FBXO22*. Western blotting was performed to detect PTEN ubiquitination levels. *P<0.05, **P<0.01 and ***P<0.001. CHX, cycloheximide; oe-, overexpression; NC, negative control.

myo-inositol levels (Fig. 7C), *IMPA1* mRNA expression and protein level (Fig. 7D and E), reduced the number of CD86-positive cells, and increased the number of CD206-positive cells (Fig. 7F and G) in mouse HCC tumors. Notably, these changes were all significantly reversed by si-*IMPA1*. These results suggested that FBXO22 upregulates myo-inositol levels, thus promoting tumor growth and inducing M2 polarization via IMPA1 in HCC tumors.

Discussion

Post-translational modifications of proteins, including glycosylation, acetylation, methylation and ubiquitination, play a key role in various cellular processes, such as signal transduction, cell proliferation, apoptosis and immune responses (17). Ubiquitination is one of the most common post-translational modifications, during which ubiquitin molecules are linked to specific target proteins by E3 ligases, initiating a cascade reaction that degrades or dysregulates target proteins. Multiple E3 ligases are closely related to tumorigenesis, and the identification of E3 ligases that target oncoproteins and tumor suppressor proteins has become a hot topic in cancer research (18,19).

In previous years, an increasing number of E3 ligases have been associated with HCC occurrence and development (20,21). FBXO22 is the F-box receptor subunit of the SCF E3 ligase that belongs to the F-box protein family (22). FBXO22 forms a

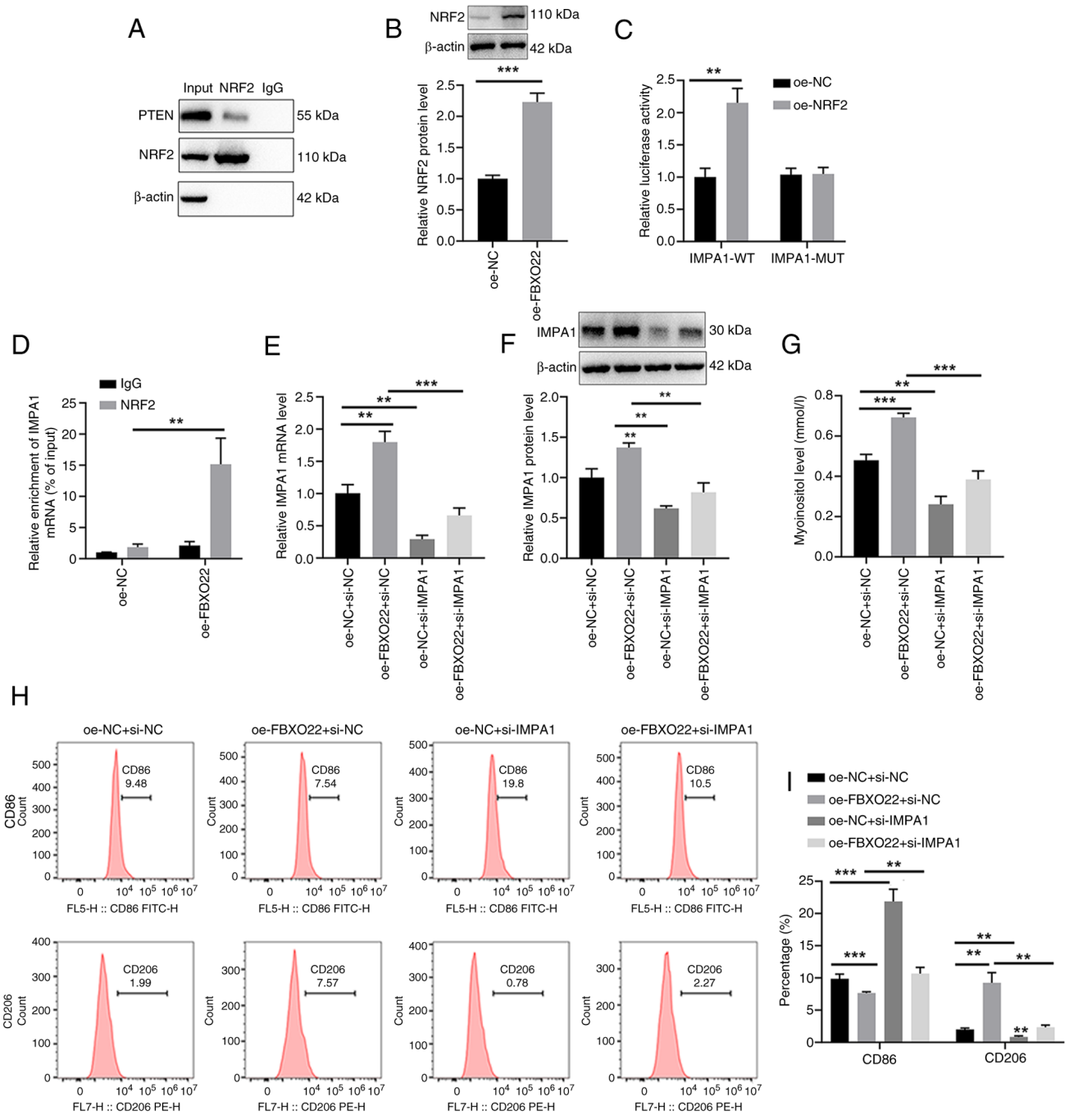

Figure 5. FBXO22-induced myo-inositol release promotes M2 polarization via the regulation of the NRF2/IMPA1 axis in THP-1 cells. (A) 97H cells were incubated with an anti-NRF2 antibody, and western blotting was performed to detect PTEN protein levels. (B) 97H cells were transfected with oe-*FBXO22*, and western blotting was performed to detect NRF2 protein level. (C) 293T cells were transfected with oe-*NRF2*, and luciferase assay was performed to determine the interaction between NRF2 and IMPA1. (D) Chromatin immunoprecipitation assay was used to detect the transcriptional regulation of IMPA1 by NRF2 in 97H cells transfected with oe-*FBXO22*, IgG was used as negative control. 97H cells were co-transfected with oe-*FBXO22* and si-*IMPA1*. (E and F) Reverse transcription-quantitative PCR and western blotting were performed to detect *IMPA1* expression. (G) A myo-inositol detect kit was used to detect myo-inositol in cell supernatants. (H and I) Flow cytometry was performed to detect CD86-positive and CD206-positive THP-1 cells. **P<0.01 and ***P<0.001. oe-, overexpression; si-, small interfering; NC, negative control.

complex with lysine demethylase to target p53 and thus plays a role in regulating body aging (23). Recently, increasing attention has been paid to the role of FBXO22 in malignant tumors. Tian *et al* (13) reported that FBXO22 promotes HCC progression by regulating the degradation of Kruppel-like factor 4. In addition, Zhang *et al* (24) reported that FBXO22 regulates the ubiquitination and degradation of p21 to promote HCC development. Zheng *et al* (25) found that FBXO22 regulates HIF-1 and VEGF impacting angiogenesis in melanoma, whereas the deletion of FBXO22 significantly inhibited migration, invasion and angiogenesis in melanoma. Lin *et al* (26) reported that FBXO22 promotes the progression of cervical cancer by targeting p57Kip2 via ubiquitination and degradation. These studies demonstrated that FBXO22 plays an important role in the occurrence and development of various tumors by regulating multiple substrate proteins. Phosphatase and tensin

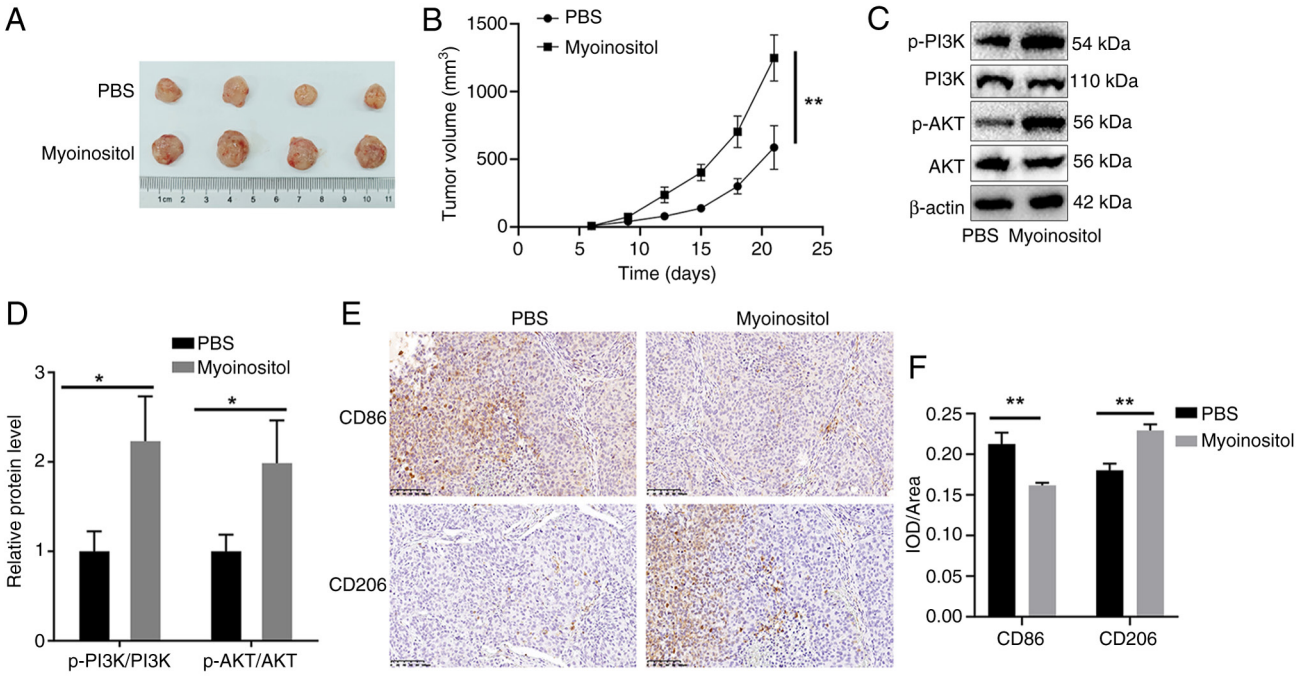

Figure 6. Myo-inositol promotes HCC tumor growth and induces M2 polarization *in vivo*. BALB/c nude mice received a subcutaneous injection of 97H cells to induce HCC. The mice were randomly divided into two groups (n=4 each): PBS group and myo-inositol group. (A and B) Tumor growth was monitored every 3 days for ~3 weeks. (C and D) Western blotting was performed to detect p-PI3K and p-AKT levels in tumor tissues. (E and F) IHC staining was performed to detect CD86-positive and CD206-positive cells in tumor tissues. *P<0.05 and **P<0.01. HCC, hepatocellular carcinoma; p-, phosphorylated.

homologue deleted on chromosome 10 (PTEN) is a known tumor suppressor expressed in various tumors, including HCC (27). Liu *et al* (28) reported that E3 ubiquitin ligase HRD1 promotes PTEN degradation by inducing its ubiquitination, thereby facilitating HCC progression. Xu *et al* (29) reported that E3 ubiquitin ligase MARCH8 promotes the malignant progression of HCC by inducing the ubiquitination and degradation of PTEN. In addition, Ge *et al* (30) reported that FBXO22 degrades nuclear PTEN to promote tumorigenesis. As expected, in the present study, FBXO22 significantly reduced PTEN protein level in HCC cells, but did not affect *PTEN* mRNA expression. Experiments with CHX and MG132 further showed that FBXO22 degraded PTEN and reduced its levels. Co-IP analysis revealed an interaction between FBXO22 and PTEN and the stimulatory effect of FBXO22 on PTEN ubiquitination in 97H cells. Increased activity of NRF2 was closely associated with PTEN loss in human carcinogenesis (31). Furthermore, there was the evidence that Nrf2 activation is influenced by PTEN/PI3K-mediated degradation (32). In the present study, co-IP analysis demonstrated a direct interaction between PTEN and NRF2 in 97H cells, and that transfection with oe-*FBXO22* upregulated NRF2 protein levels in 97H cells. Thus, it was hypothesized that FBXO22 degrades PTEN by inducing PTEN ubiquitination, which upregulated NRF2 protein levels in HCC cells. In addition, *in vivo* experiments revealed the promoting effect of FBXO22 on tumor growth and M2-type macrophages in HCC mice, although the mechanisms underlying these effects are unclear. Actually, the increased FBXO22 level also correlated strongly with a poor prognosis in patients with HCC (24,33). However, in the present study, the clinical analysis of FBXO22 was not conducted.

In addition to classical stimuli, macrophage differentiation is determined by redundant factors in parenchymal cells. HGF induces M2 polarization of macrophages, promoting tumor progression by participating in the anti-inflammatory response in various tissues (34). Zhao *et al* (35) reported that miR-144/miR-451a overexpression stimulated M1 polarization of macrophages by reducing the secretion of HGF and MIF by HCC cells, thus activating cytotoxic T lymphocytes. Thus, it was wondered whether FBXO22 induces M2 polarization of macrophages to promote HCC progression via paracrine factors. Thus, in the present study, non-targeted metabolomic analysis of 97H cells transfected with oe-*FBXO22* was performed, and myo-inositol was selected for subsequent experiments. Myo-inositol is a ubiquitous compound found in all living organisms and reduction in myo-inositol was shown to affect PI3K-dependent inhibition of programmed cell death (36). Antony *et al* (37) reported that myo-inositol stimulated adipocyte differentiation via increasing PPAR-γ expression and enhanced insulin receptor signaling via the PI3K/p-Akt pathway in adipose tissues. Jiang *et al* (38) reported that supplementation with dietary myo-inositol increased white blood cell counts and improved phagocytosis of leucocytes in fish. Ghosh *et al* (39) reported that myo-inositol in fermented sugar matrix improves macrophage function for host defense against invading pathogens. An *in vivo* experiment on lung cancer revealed that the combination of myo-inositol and chemo-preventive agents increases the infiltration of lung tumors by $CD4^+$ and $CD8^+$ T cells (40). Additionally, a clinical study revealed that the higher myo-inositol in the temporal lobes of patients with temporal lobe epilepsy is associated with a higher frequency of $CD4^+$T-cell and $CD19^+$B-cell subsets (41). However, myo-inositol was neurotoxic to

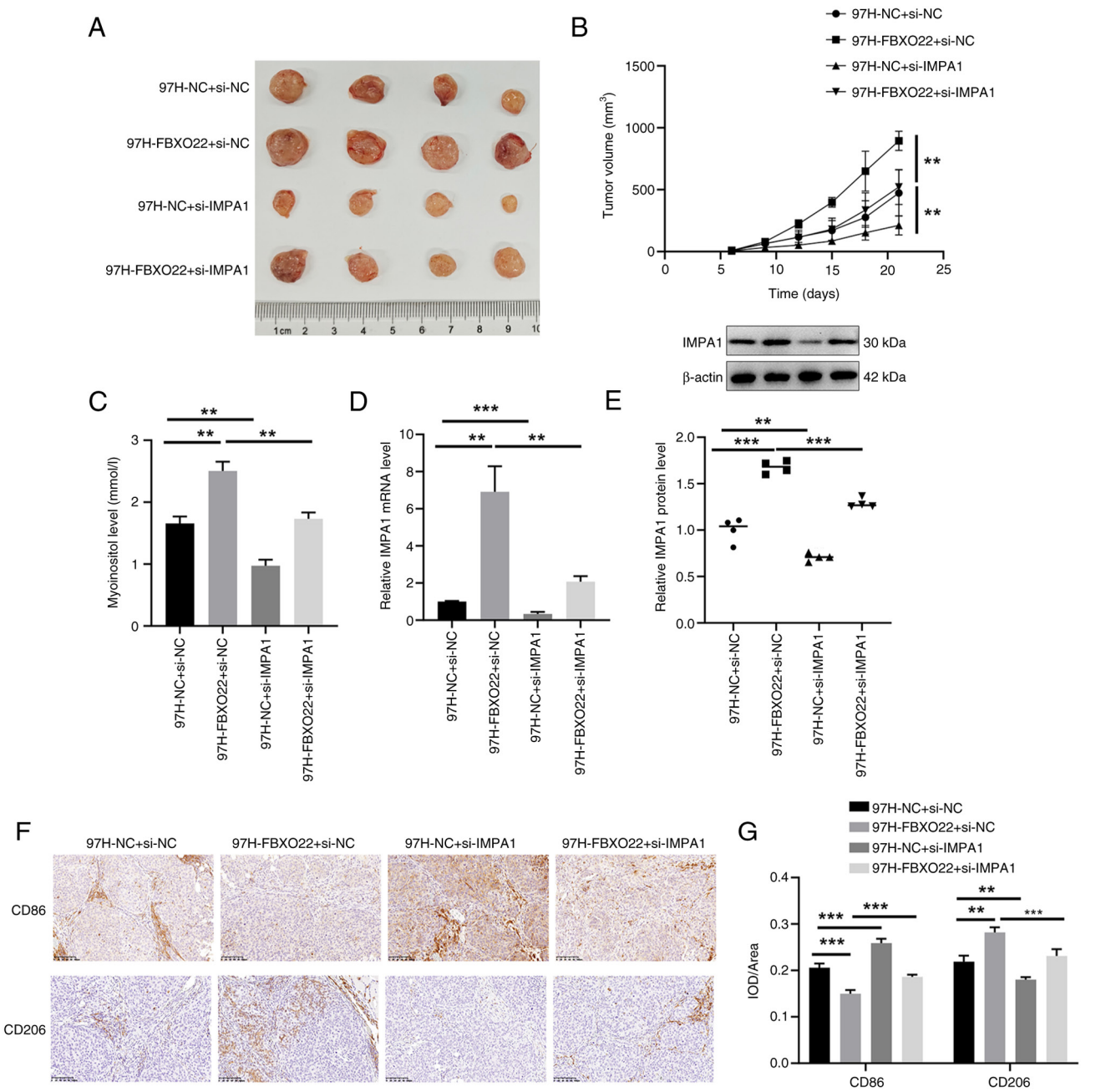

Figure 7. Transfection with si-*IMPA1* reverses the stimulatory effect of FBXO22 on tumor growth and M2 polarization *in vivo*. BALB/c nude mice were subcutaneously injected with 97H cells to induce hepatocellular carcinoma. The model mice were randomly divided into four groups (n=4 each): 97H-NC + si-NC, 97H-FBXO22 + si-NC, 97H-NC + si-IMPA1, and 97H-FBXO22 + si-IMPA1. (A and B) Tumor growth was monitored every 3 days for ~3 weeks. (C) A myo-inositol detection kit was used to detect myo-inositol in tumor tissues. (D) Reverse transcription-quantitative PCR was performed to detect IMPA1 mRNA expression in tumor tissues. (E) Western blotting was performed to detect IMPA1 protein level in tumor tissues. (F and G) IHC staining was performed to detect CD86-positive and CD206-positive cells in tumor tissues. **P<0.01 and ***P<0.001. si-, small interfering; NC, negative control.

Schwann cells (42). In the present study, myo-inositol was found to be non-toxic to 97H cells. The PI3K/AKT pathway is involved in the inflammatory response and affects macrophage polarization, proliferation and migration. AKT is activated via the phosphorylation by PI3K, which induces M2-type macrophages to attenuate inflammatory response (43,44). As expected, myo-inositol activated the PI3K/AKT pathway and induced M2-type polarization of THP-1 cells. Given that both these effects were markedly reversed by transfection with si-*SLC5A3*, it can be concluded that SLC5A3 participates in the promoting effect of myo-inositol on M2 polarization.

IMPA1 catalysis is the rate-limiting step in myo-inositol synthesis. In the present study, considering the higher transfection efficiency of 293T cells, the luciferase assay was performed in 293T cells to reveal that NRF2 directly bound to *IMPA1* mRNA. Furthermore, to better understand the interaction between NRF2 and IMPA1 in HCC, 97H cells were employed for ChIP assay, and the direct transcriptional regulation of *IMPA1* by NRF2 was observed in 97H cells. Transfection with oe-*FBXO22* elevated NRF2 protein levels in 97H cells. In addition, the increased IMPA1 expression and myo-inositol release induced by the treatment with oe-*FBXO22* were reversed

by si-*IMPA1* in 97H cells, suggesting that FBXO22 induced myo-inositol release in HCC cells via the NRF2/IMPA1 axis. Furthermore, the increase in the number of M2-type macrophages induced by 97H cells transfected with oe-*FBXO22* was reversed by the co-transfection with si-*IMPA1*. *In vivo* experiments further confirmed that the stimulatory effect of myo-inositol on tumor growth and M2-type macrophages in HCC was associated with the FBXO22/IMPA1 axis.

In summary, the results of the present study demonstrated that FBXO22 degraded PTEN by inducing its ubiquitination, which upregulated NRF2 protein expression. This, in turn, stimulated IMPA1 to induce myo-inositol release by HCC cells. The resulting induction of M2-type polarization in macrophages via SLC5A3 promoted HCC tumor growth. However, the therapeutic targets of the FBXO22/myo-inositol relationship *in vivo* remained unexplored and require further investigation.

Acknowledgements

Not applicable.

Funding

The present study was supported by the Training Program for Academic and Technical Leaders in Major Disciplines-Young Talents (grant no. 20232BCJ23039), the National Natural Science Foundation of China (grant nos. 82260514, 82160095 and 82003121), the Natural Science Foundation of Jiangxi (grant nos. 20224ACB206001 and 20242BAB20409), the Key Laboratory Project of Digestive Diseases in Jiangxi (grant no. 2024SSY06101) and the Jiangxi Clinical Research Center for Gastroenterology (grant no. 20223BCG74011).

Availability of data and materials

The data generated in the present study may be requested from the corresponding author.

Authors' contributions

LLB, JX and SHC contributed to the conception and main experiments of the present study and wrote the draft of the manuscript. JHH performed the *in vitro* experiments. MXZ, BML and JH contributed to analysis and interpretation of data. MYH contributed to acquisition of data, revised the article and provided software and resources. LLB and MYH confirm the authenticity of all the raw data. All authors read and approved the final version of the manuscript

Ethics approval and consent to participate

The present study was approved by the Institutional Animal Care and Use Committee of the First Affiliated Hospital, Jiangxi Medical College, Nanchang University (approval no. CDYFY-IACUC-202501GR136; Nanchang, China).

Patient consent for publication

Not applicable.

Competing interests

The authors declare that they have no competing interests.

References

1. Ferenci P, Fried M, Labrecque D, *et al*: Hepatocellular carcinoma (HCC): A global perspective. Arab Journal of Gastroenterology 11: 174-179, 2010.
2. Brown ZJ, Tsilimigras DI, Ruff SM, Mohseni A, Kamel IR, Cloyd JM and Pawlik TM: Management of hepatocellular carcinoma A review. JAMA Surg 158: 410-420, 2023.
3. Vitale I, Manic G, Coussens LM, Kroemer G and Galluzzi L: Macrophages and metabolism in the tumor microenvironment. Cell Metab 30: 36-50, 2019.
4. Hinshaw DC and Shevde LA: The tumor microenvironment innately modulates cancer progression. Cancer Res 79: 4557-4566, 2019.
5. Li Z, Wu T, Zheng B and Chen L: Individualized precision treatment: Targeting TAM in HCC. Cancer Lett 458: 86-91, 2019.
6. Du M, Sun L, Guo J and Lv H: Macrophages and tumor-associated macrophages in the senescent microenvironment: From immunosuppressive TME to targeted tumor therapy. Pharmacol Res 204: 107198, 2024.
7. Christofides A, Strauss L, Yeo AT, Cao C, Charest A and Boussiotis V: The complex role of tumor-infiltrating macrophages. Nat Immunol 23: 1148-1156, 2022.
8. Yang T, Wang Y, Dai W, Zheng X, Wang J, Song S, Fang L, Zhou J, Wu W and Gu J: Increased B3GALNT2 in hepatocellular carcinoma promotes macrophage recruitment via reducing acetoacetate secretion and elevating MIF activity. J Hematol Oncol 11: 50, 2018.
9. Shiau DJ, Kuo WT, Davuluri GVN, Shieh CC, Tsai PJ, Chen CC, Lin YS, Wu YZ, Hsiao YP and Chang CP: Hepatocellular carcinoma-derived high mobility group box 1 triggers M2 macrophage polarization via a TLR2/NOX2/autophagy axis. Sci Rep 10: 13582, 2020.
10. Nguyen KM and Busino L: The biology of F-box proteins: The SCF family of E3 ubiquitin ligases. Adv Exp Med Biol 1217: 111-122, 2020.
11. Ho MS, Tsai PI and Chien CT: F-box proteins: The key to protein degradation. J Biomed Sci 13: 181-191, 2006.
12. Tan MKM, Lim HJ and Harper JW: SCFFBXO22 regulates histone H3 lysine 9 and 36 methylation levels by targeting histone demethylase KDM4A for ubiquitin-mediated proteasomal degradation. Mol Cell Biol 31: 3687-3699, 2011.
13. Tian X, Dai S, Sun J, Jin G, Jiang Y, Meng F, Li Y, Wu D and Jiang Y: F-box protein FBXO22 mediates polyubiquitination and degradation of KLF4 to promote hepatocellular carcinoma progression. Oncotarget 6: 22767-22775, 2015.
14. Livak KJ and Schmittgen TD: Analysis of relative gene expression data using real-time quantitative PCR and the 2(-Delta Delta C(T)) method. Methods 25: 402-408, 2001.
15. Croze ML, Vella RE, Pillon NJ, Soula HA, Hadji L, Guichardant M and Soulage CO: Chronic treatment with myo-inositol reduces white adipose tissue accretion and improves insulin sensitivity in female mice. J Nutr Biochem 24: 457-466, 2013.
16. Food and Drug Administration (FDA): Estimating the Maximum Safe Starting Dose in Initial Clinical Trials for Therapeutics in Adult Healthy Volunteers. FDA, Rockville, MD, 2005.
17. Toit AD: Post-translational modification: Sweetening protein quality control. Nat Rev Mol Cell Biol 15: 295, 2014.
18. Wang S, Osgood AO and Chatterjee A: Uncovering post-translational modification-associated protein-protein interactions. Curr Opin Struct Biol 74: 102352, 2022.
19. Park J, Cho J and Song EJ: Ubiquitin-proteasome system (UPS) as a target for anticancer treatment. Arch Pharm Res 43: 1144-1161, 2020.
20. Brauckhoff A, Ehemann V, Schirmacher P and Breuhahn K: Reduced expression of the E3-ubiquitin ligase seven in absentia homologue (SIAH)-1 in human hepatocellular carcinoma. Verh Dtsch Ges Pathol 91: 269-277, 2007 (In German).
21. Lin XT, Zhang J, Liu ZY, Wu D, Fang L, Li CM, Yu HQ and Xie CM: Elevated FBXW10 drives hepatocellular carcinoma tumorigenesis via AR-VRK2 phosphorylation-dependent GAPDH ubiquitination in male transgenic mice. Cell Rep 42: 112812, 2023.
22. Kipreos ET and Pagano M: The F-box protein family. Genome Biol 1: 1-7, 2000.

23. Johmura Y, Sun J, Kitagawa K, Nakanishi K, Kuno T, Naiki-Ito A, Sawada Y, Miyamoto T, Okabe A, Aburatani H, *et al*: SCFFbxo22-KDM4A targets methylated p53 for degradation and regulates senescence. Nat Commun 7: 10574, 2016.
24. Zhang L, Chen J, Ning D, Liu Q, Wang C, Zhang Z, Chu L, Yu C, Liang HF, Zhang B and Chen X: FBXO22 promotes the development of hepatocellular carcinoma by regulating the ubiquitination and degradation of p21. J Exp Clin Cancer Res 38: 101, 2019.
25. Zheng Y, Chen H, Zhao Y, Zhang X, Liu J, Pan Y, Bai J and Zhang H: Knockdown of FBXO22 inhibits melanoma cell migration, invasion and angiogenesis via the HIF-1α/VEGF pathway. Invest New Drugs 38: 20-28, 2020.
26. Lin M, Zhang J, Bouamar H, Wang Z, Sun LZ and Zhu X: Fbxo22 promotes cervical cancer progression via targeting p57Kip2 for ubiquitination and degradation. Cell Death Dis 13: 805, 2022.
27. Dahia PL: PTEN, a unique tumor suppressor gene. Endocr Relat Cancer 7: 115-129, 2000.
28. Liu L, Long H, Wu Y, Li H, Dong L, Zhong JL, Liu Z, Yang X, Dai X, Shi L, *et al*: HRD1-mediated PTEN degradation promotes cell proliferation and hepatocellular carcinoma progression. Cell Signal 50: 90-99, 2018.
29. Xu Y, Zhang D, Ji J and Zhang L: Ubiquitin ligase MARCH8 promotes the malignant progression of hepatocellular carcinoma through PTEN ubiquitination and degradation. Mol Carcinog 62: 1062-1072, 2023.
30. Ge MK, Zhang N, Xia L, Zhang C, Dong SS, Li ZM, Ji Y, Zheng MH, Sun J, Chen GQ and Shen SM: FBXO22 degrades nuclear PTEN to promote tumorigenesis. Nat Commun 11: 1720, 2020.
31. Rojo AI, Rada P, Mendiola M, Ortega-Molina A, Wojdyla K, Rogowska-Wrzesinska A, Hardisson D, Serrano M and Cuadrado A: The PTEN/NRF2 axis promotes human carcinogenesis. Antioxid Redox Signal 21: 2498-2514, 2014.
32. Ding C, Zou Q, Wu Y, Lu J, Qian C, Li H and Huang B: EGF released from human placental mesenchymal stem cells improves premature ovarian insufficiency via NRF2/HO-1 activation. Aging (Albany NY) 12: 2992-3009, 2020.
33. Lei Z, Luo Y, Lu J, Fu Q, Wang C, Chen Q, Zhang Z and Zhang L: FBXO22 promotes HCC angiogenesis and metastasis via RPS5/AKT/HIF-1α/VEGF-A signaling axis. Cancer Gene Ther 32: 198-213, 2025.
34. Choi W, Lee J, Lee J, Lee SH and Kim S: Hepatocyte growth factor regulates macrophage transition to the M2 Phenotype and promotes murine skeletal muscle regeneration. Front Physiol 10: 914, 2019.
35. Zhao J, Li H, Zhao S, Wang E, Zhu J, Feng D, Zhu Y, Dou W, Fan Q, Hu J, *et al*: Epigenetic silencing of miR-144/451a cluster contributes to HCC progression via paracrine HGF/MIF-mediated TAM remodeling. Mol Cancer 20: 46, 2021.
36. Meng PH, Raynaud C, Tcherkez G, Blanchet S, Massoud K, Domenichini S, Henry Y, Soubigou-Taconnat L, Lelarge-Trouverie C, Saindrenan P, *et al*: Crosstalks between Myo-Inositol metabolism, programmed cell death and basal immunity in arabidopsis. PLoS One 4: e7364, 2009.
37. Antony PJ, Gandhi GR, Stalin A, Balakrishna K, Toppo E, Sivasankaran K, Ignacimuthu S and Al-Dhabi NA: Myoinositol ameliorates high-fat diet and streptozotocin-induced diabetes in rats through promoting insulin receptor signaling. Biomed Pharmacother 88: 1098-1113, 2017.
38. Jiang WD, Feng L, Liu Y, *et al*: Effects of graded levels of dietary myo-inositol on non-specific immune and specific immune parameters in juvenile Jian carp (Cyprinus carpio var. Jian). Aquaculture Research 41: 1413-1420, 2010.
39. Ghosh N, Das A, Biswas N, Mahajan SP, Madeshiya AK, Khanna S, Sen CK and Roy S: Myo-inositol in fermented sugar matrix improves human macrophage function. Mol Nutr Food Res 66: e2100852, 2022.
40. Kassie F, Bagherpoor AJ, Kovacs K and Seelig D: Combinatory lung tumor inhibition by myo-inositol and iloprost/rapamycin: Association with immunomodulation. Carcinogenesis 43: 547-556, 2022.
41. Mueller C, Hong H, Sharma AA, Qin H, Benveniste EN and Szaflarski JP: Brain temperature, brain metabolites, and immune system phenotypes in temporal lobe epilepsy. Epilepsia Open 9: 2454-2466, 2024.
42. Niwa T, Sobue G, Maeda K and Mitsuma T: Myoinositol inhibits proliferation of cultured Schwann cells: Evidence for neurotoxicity of myoinositol. Nephrol Dial Transplant 4: 662-666, 1989.
43. Hofmann BT and Jücker M: Activation of PI3K/Akt signaling by n-terminal SH2 domain mutants of the p85α regulatory subunit of PI3K is enhanced by deletion of its c-terminal SH2 domain. Cell Signal 24: 1950-1954, 2012.
44. Baitsch D, Bock HH, Engel T, Telgmann R, Müller-Tidow C, Varga G, Bot M, Herz J, Robenek H, von Eckardstein A and Nofer JR: Apolipoprotein E induces antiinflammatory phenotype in macrophages. Arterioscler Thromb Vasc Biol 31: 1160-1168, 2011.